11th International Workshop on Ship and Marine Hydrodynamics
Hamburg, Germany, September 22-25, 2019

Development of Air Lubrication System for Reduction of Ship Frictional Drag

Sangmin Kim[1,*], Jinhak Kim[1], Soonho Choi[1]

[1] Samsung Heavy Industries Co. Ltd., Samsung Ship Model Basin
217 Munji-ro, Yuseong-gu, Daejeon 305-380, Korea

*Corresponding author, shism.kim@samsung.com

ABSTRACT

Frictional resistance occupies a large portion of the total resistance of a vessel accounting for nearly 60 ~ 80%, and reducing friction resistance can lead to a remarkable reduction in greenhouse gas (GHG) emissions from ships. Air lubrication method is widely recognized as one of the useful technologies to reduce a ship's frictional resistance by injecting air to cover a large portion of wetted hull surface. In present study, firstly, the effects of injected air layer on the skin frictional drag are investigated through various experiments and relevant analysis on a flat plate and model ships. Then, particular air lubrication systems (ALS) for two full scale ships are designed, and their performance are validated by the data obtained during actual voyages. A heavy cargo carrier and an LNG carrier are selected for the full scale applications. The amount of fuel saving through the application of the air lubrication system is evaluated by analysing operation data acquired during sea trials and actual voyages in service. The installed air lubrication system on the bottom of the ship hull is found to be effective for the reduction of the fuel oil consumption. The overall efficiency of the air lubrication system can be further improved by optimizing size and location of the air injectors, which are deemed as the two important parameters for optimum design of the air lubrication system. This paper discusses the experience gained in applying the air lubrication technology to the full scale ships, and demonstrates the effectiveness of the air lubrication for reducing fuel consumption of ships

1 INTRODUCTION

In order to reduce the operating costs of a vessel and meet the Energy Efficiency Design Index (EEDI) regulations of International Maritime Organization (IMO) on greenhouse gas (GHG) emissions from vessels, many maritime research institutes have developed energy saving devices. The air lubrication system is one of the ESD (Energy Saving Device) that injects air into the bottom of the hull to form an air layer between the hull surface and sea water through which the ship's frictional resistance can be reduced.

Proactive efforts have been made to develop air lubrication systems (hereafter ALS) for transoceanic commercial vessels especially in Japan and Europe. In the meantime, Samsung Heavy Industries (SHI) has been developing its own air lubrication system in a systematic manner.

In this paper, the design and calibration of the ALS designed by SHI for the two full scale ships in conjunction with model test results are introduced, and the power savings of the ALS are evaluated by performing the analysis through sea trials and long-term voyages in service in comparison with the power saving effect estimated by model tests.

2 BASIC RESEARCH

2.1 Feasibility Study of Drag Reduction by Air Injection

When air is injected on the bottom surface of a ship hull, the air stream breaks into pieces and forms an air-water mixture flow consisting of air bubbles and water. When the injected air flow rate is continuously increased, some bubbles merge together to form a partial air layer. Eventually, a transitional air layer is formed in the area where a mixed flow of bubbles and continuous air layer coexist. The frictional drag on the hull surface with continuous air layer is then reduced effectively as if the wetted surface area is reduced by replacing the skin friction between water and hull surface with that between air and hull [1]. Elbing suggests that the transitional air layer can reduce the local frictional drag by 20% to 80% [2]. When the injected air flow rate is further increased to exceed a critical value, the merging of bubbles is promoted to form a substantially continuous large scale air layer as shown in Fig. 1. In such a case, the reduction of the local frictional drag is expected to be about 80% or more.

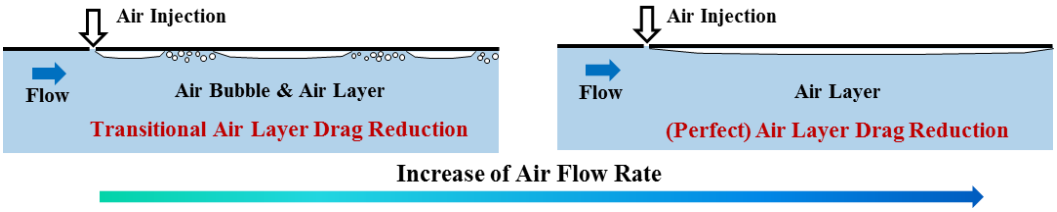

Figure 1: Schematic figures of drag reduction due to air layer

In order to investigate the characteristics of the air layer and estimate quantitative reduction rate of the frictional drag, a set of experiment was conducted to simulate an air layer formed on a flat bottom as shown in Fig. 2. Air was injected at various flow rates onto the bottom of a flat plate to form an air layer at various water inflow speeds after the plate was mounted horizontally.

Figure 2: Flat plate installed in the cavitation tunnel at SSMB

Figure 3 shows the frictional drag reduction rate of the flat plate with thickness of the air layers at water inflow speed of 5 m/s, where the thickness of the air layer is defined as follows:

$$t_{AL} = \frac{Q_{Air}}{V \cdot B_{Air}} \quad . \tag{1}$$

In the Eq. (1), Q_{Air} is the volumetric flow rate of the injected air that is converted at the pressure of the test section from the measured air flow rate in normal condition of 1 atm and 0°C. Here, V and B_{Air} denote water inflow velocity and the width of the air injection slit, respectively. Therefore, t_{AL} means the ideal air layer thickness obtained under the assumption that the air layer is formed with the same width of the air injection slit. As displayed in Fig. 3, the reduction rate of the frictional drag increases with the thickness of the air layer, and converges to the maximum rate of 90% at $t_{AL} \approx 10$mm. Through a series of experiments, it has been verified at a laboratory scale that the reduction of frictional drag of ships by ALS is feasible. The experimental results were used as baseline data for the basic design of the ALS for applications to the full scale ships.

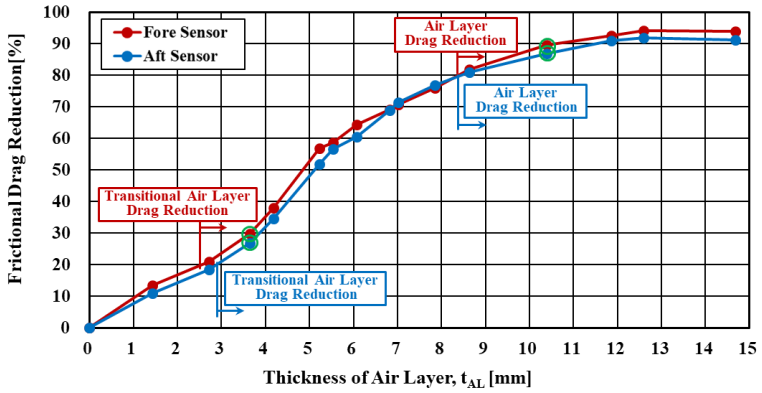

Figure 3: SSMB Frictional drag reduction by air flow rate (V=5m/s)

2.2 Performance Estimation Method of ALS by Model Tests

In the previous studies on ALS, SHI has proposed a performance estimation method of net power saving based on model test results [3]. According to the study, the effective power of a full scale ship can be estimated assuming that the air injection does not influence the residuary resistance, and the frictional drag reduction ratio of the full scale is equal to that of the model scale. Based on these assumptions, the total resistance and effective power of the full scale ship can be estimated as follows [7]:

Case without air injection:

$$C_{TS} = \left(\frac{S + S_{BK}}{S} \right) \left(C_{FS} + C_A \right) + C_R + C_{AA} \tag{2}$$

$$P_E = R_{TS} \cdot V_S \tag{3}$$

Case with air injection:

$$C_{R,Air} = C_R \tag{4}$$

$$C_{FM,Air} = C_{TM,Air} - C_R \tag{5}$$

$$\frac{C_{FM,Air}}{C_{FM}} = \frac{C_{FS,Air}}{C_{FS}} \tag{6}$$

$$C_{TS,Air} = \left(\frac{S + S_{BK}}{S} \right) \left(C_{FS,Air} + C_A \right) + C_{R,Air} + C_{AA} \tag{7}$$

$$P_{E,Air} = R_{TS,Air} \cdot V_S \tag{8}$$

Here, the subscripts "*M*" and "*S*" in Eq. (2) ~ (8) denote the values at model scale and full scale, respectively. Subscript "Air" means the value in the case of air injection. C_T is the total resistance coefficient, C_F is the frictional resistance coefficient obtained from ITTC 1957 model-ship correlation line, C_A is the model-ship correlation allowance coefficient, C_R is the residuary resistance coefficient, C_{AA} is the air resistance coefficient in head wind, S is the wetted surface area of the hull, S_{BK} is the wetted surface area of bilge keels, P_E is the effective power, R_T is the total resistance, and V is the ship speed.

In estimating delivered power, the full scale wake fraction and the full scale resistance coefficient in the case of air injection are calculated by the following Eq. (12), (13), and (14) using the values derived from the effective power estimation above. The other coefficients can be obtained by the same method without air injection. The delivered power can be obtained using the coefficients according to the presence or absence of the air injection.

Case without air injection:

$$F_D = \frac{1}{2}\rho_M S_M V_M{}^2 \cdot \{C_{FM} - (C_{FS} + C_A)\} \tag{9}$$

$$w_{TS} = (t + 0.04) + (w_{TM} - t - 0.04)\frac{C_{FS} + C_A}{C} \tag{10}$$

$$\left(\frac{K_T}{J^2}\right) = \frac{S}{2D^2}\frac{C_{TS}}{(1-t)(1-w_{TS})^2} \tag{11}$$

Case with air injection:

$$F_D = \frac{1}{2}\rho_M S_M V_M{}^2 \cdot \{C_{FM,Air} - (C_{FS,Air} + C_A)\} \tag{12}$$

$$w_{TS,Air} = (t_{Air} + 0.04) + (w_{TM,Air} - t_{Air} - 0.04)\frac{C_{FS,Air} + C_A}{C_{FM,Air}} \tag{13}$$

$$\left(\frac{K_T}{J^2}\right)_{Air} = \frac{S}{2D^2}\frac{C_{TS,Air}}{(1-t_{Air})(1-w_{TS,Air})^2} \tag{14}$$

Here, F_D is the towing force in a self-propulsion test, t is the thrust reduction fraction, w_T is the effective wake fraction, K_T/J^2 is the loading coefficient of the full scale propeller, and D is the propeller diameter. The definitions of the other variables and subscripts are the same as those used in the previous equations.

Finally, the net power saving is obtained by subtracting the power required for air injection from the difference of delivered powers with and without air injection. In such case, the required flow rate of the injected air is calculated from the air layer thickness, $t_{AL,}$ which is given in Eq.(1) in the standard condition ($25°C$, 1 *atm*) under the assumption that the air layer thickness maintains the same level in both the model scale and the full scale. The required power for the air injection (i.e. air compressor horsepower) is estimated to be the power spent to compress a given quantity of air in the standard condition via a polytropic process as shown in the following Eq. (15) [4~6].

$$P_{Air} = \frac{Q_{SAir}}{\eta_C} \cdot p_1 \cdot \frac{n}{(n-1)} \cdot \left\{\left(\frac{p_2}{p_1}\right)^{\frac{(n-1)}{n}} - 1\right\} \tag{15}$$

In the equation above, P_{Air} is the power required for air injection, Q_{SAir} is the full scale flow rate of injected air in the standard condition, η_C is the efficiency of the air compressor (or blower), n is the polytropic index, p_1 is the atmospheric pressure and p_2 is the pressure of the compressed air to be injected on the bottom of the hull. In this study, the efficiency, η_C, of the air compressor is assumed to be 0.6, and the value of polytropic index, n, is assumed to be 1.4 corresponding to the adiabatic process.

2.3 Performance Estimation for Heavy Cargo Carrier

It is generally acknowledged in the shipbuilding industry that ships suitable to apply ALS is wide-beam, shallow draught vessels. One of the vessels selected for the development of full scale prototype was a Heavy Cargo Carrier (HCC), transporting ship blocks from Rongcheng, China to Geoje, South Korea. The optimal flow rate of injected air and power saving performance were estimated through towing tank model tests with and without air injection at SSMB. The principal particulars and pictures of the model ship are shown in Table 1 and Fig. 4, respectively.

Table 1: Principal Particulars of Heavy Cargo Carrier

Principal Particulars	
Length overall	165.0 m
Breadth	42.0 m
Design Draught(Td)	5.25 m
Flat Bottom Area (% of WSA at Td)	48.3 %

Based on the results given in the previous study [3], two rows of air injectors were arranged in the forward part of the HCC, resulting in larger power saving and more stable air layer pattern even in moderate head sea conditions. The required flow rate of the injected air and quantitative power saving were estimated through three stages of optimization processes according to the aforementioned performance estimation method.

First, a resistance test is conducted at a towing tank to find the optimal flow rate of the injected air at the first row location (FWD1) for the purpose of achieving the largest drag reduction. Fig. 5 presents the variation of ΔRTM (i.e. the difference between the total resistance with and without air injection in model scale) along with air layer thickness.

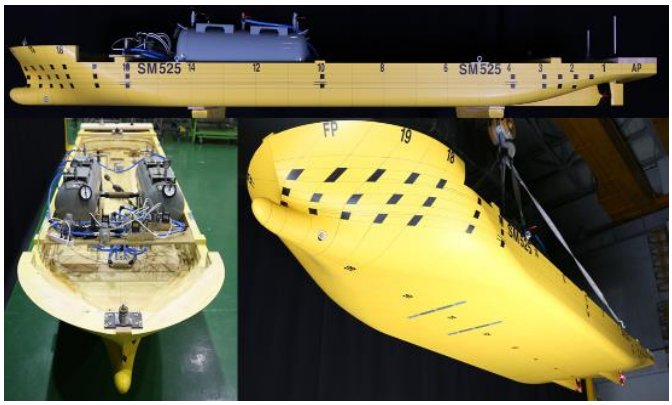

Figure 4: Model ship of heavy cargo carrier

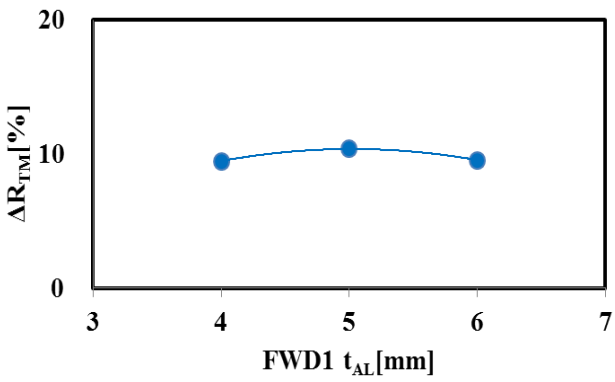

Figure 5: Resistance variation with air flow rate (FWD1)

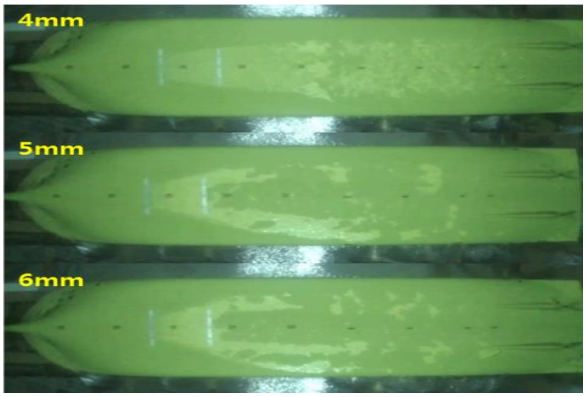

Figure 6: Behaviour of injected air from FWD1 injectors

The behaviour of the air layer formed on the flat bottom area under various air layer thickness conditions (i.e. air flow rates) are illustrated in Fig. 6. It indicates that the injected air with air layer thickness over 4*mm* is not noticeable along the flow direction and spreads to the sides in the beam direction. Furthermore, it can be noted that the resistance reduction does not increase in proportion to the flow rate when the air layer thickness is over 4*mm*. Therefore, the optimal thickness of the injected air is determined to be $t_{AL} \approx 4mm$.

The next step is to find the optimal flow rate of injected air at the second row location (FWD2). While the air layer thickness of the FWD1 is fixed to be 4*mm*, measured resistance and behaviour of the injected air depending on air layer thickness of FWD2 are shown in Fig. 7 and 8, respectively. It is shown in Fig. 7 that the resistance reduction does not increase further even at increased air flow rate when the air layer thickness exceeds 4 (from FWD1) + 15 (from FWD2)*mm*. In addition, the injected air starts to spread to the sides as the air layer thickness is increased to reach 4 + 15*mm*. Based on the observation above, the optimal air layer thickness of the HCC was determined to be 4 + 13*mm*.

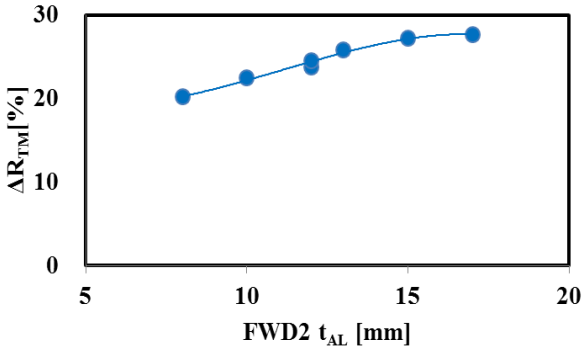

Figure 7: Resistance variation with air flow rate (FWD1 & 2)

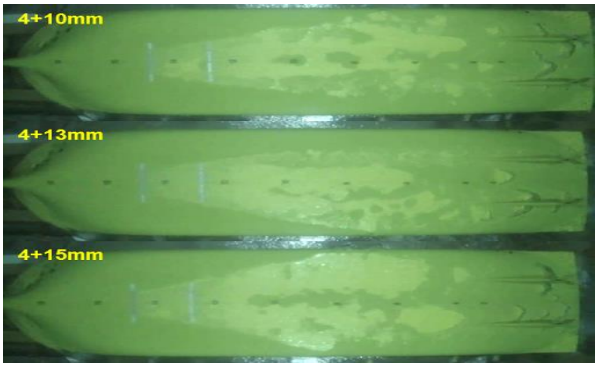

Figure 8: Behaviour of injected air from FWD1 & FWD2 injectors

Finally, a series of resistance and self-propulsion tests are carried out to evaluate the power savings of the vessel at the determined air flow rate. Fig. 9 shows the rates of change in various powers with air injection relative to those without air injection at design draught, such as effective power (PE), shaft power (PS), power required for air injection (PA) and net power (PNET). Table 2 summarizes the measured power savings at the ship speed of 12 knots with respect to required powers without air injection at design and ballast draughts, respectively.

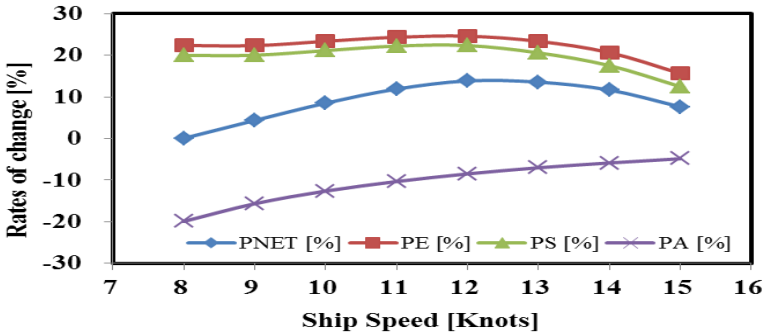

Figure 9: Evaluated power saving performance in model test (HCC)

Table 2: Model test results for HCC at 12knots

Item	Design	Ballast
Effective Power Reduction	24.6%	26.1%
Shaft Power Reduction	22.3%	24.5%
Required Power for Air Supply	8.5%	8.8%
Net Power Saving	13.8%	15.7%

[Net Power Saving] = [Power Saving] - [Required Power for Air Supply]

2.4 Performance Estimation for LNG Carrier

The hydrodynamics of twin skeg ships is characterized by the flow pattern along the buttock line between two stern skegs. The air injected from the fore part of the ship also flows to the stern region without spreading to the sides so that additional drag reduction can be achieved by air layer on the stern area between skegs. For this reason, 170K class twin skeg LNG carrier was selected to estimate the performance of the ALS. Similar to the case of HCC, the model tests for air flow rate optimization and performance evaluation were conducted at SSMB. The selected LNG carrier, whose principal dimensions are summarized in Table 3, was constructed and delivered by SHI in 2010. The flat bottom area occupied about 41% of the total wetted surface area, which was expected to have a significant effect on the reduction of the frictional resistance.

However, the air layer was not expected to cover most of the wetted surface areas, since air injectors were planned to be placed only inside the pipe duct on the center line of the ship due to limited space and technical risks of retrofit work. As illustrated in Fig. 10, air injectors were arranged in three rows including two rows in the forward part and one row in the aft part, and the air flow rates of each row of injectors were optimized at the operation speed of 17.5 knots [8].

Table 3: Principal dimensions of 170K class LNGC

Principal dimensions	
Length Overall	290m
Breadth (B)	45m
Draught (T)	11.5m
Flat Bottom Area / WSA	40.5%

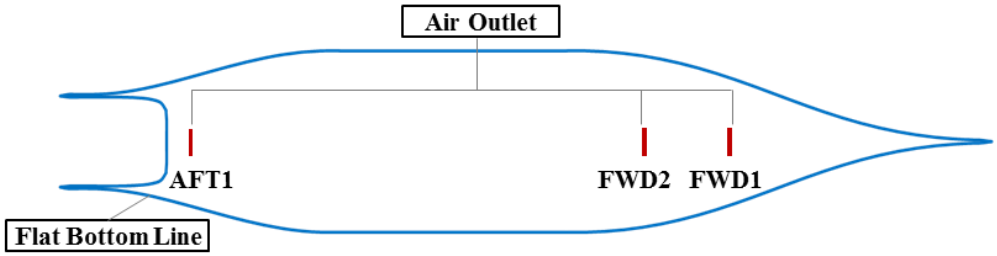

Figure 10: Arrangement of air injectors for 170K Class LNGC

The optimal combination of air layer thicknesses among the rows was found to be 5 (FWD1) + 9 (FWD2) + 5 (AFT1)*mm* through model tests. The behaviour of the air layer formed on the bottom of the model ship is shown in Fig. 11. Figure 12 indicates the measured power savings at various ship speeds. At the ship speed of 17.5 knots, 6% and 8% of the net power savings were estimated at the design and ballast draught conditions, respectively, as presented in Table 4.

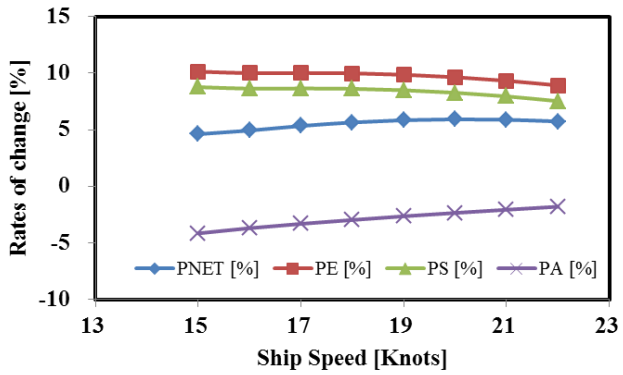

Figure 11: Evaluated power performance at model test (LNGC)

Figure 12: Snapshot of air layer on LNGC (17.5 knots)

Table 4: Model test results for 170K LNGC (at 17.5knots)

Item	Design	Ballast
Effective Power Reduction	10.0%	12.0%
Shaft Power Reduction	9.0%	11.0%
Required Power for Air Supply	3.0%	3.0%
Net Power Saving	6.0%	8.0%

[Net Power Saving] = [Power Saving] - [Required Power for Air Supply]

3 EQUIPMENTS AND INSTALLATION

Based on the design parameters obtained from the model tests and optimization process described above, the detailed design of the prototype of the ALS was carried out to apply to the two ships.

3.1 System Arrangement

Figure 13 shows the arrangement of the main equipment constituting the ALS. Due to the limited installation space, the air compressor of the HCC was installed on the upper deck, and the water cooling pump was installed underneath to supply cooling water from the sea chest to the compressor.

In the case of LNGC, two compressors were installed in bosun store and engine room, respectively. The compressor in the bosun store supplies air to two rows of air injectors in the forward part as well as that in the engine room to single row of air injectors in the aft part. A booster pump was installed to supply cooling water to each compressor from the stern sea chest. The ALS controllers of HCC and LNGC were designed to monitor the operating condition and inject air at the optimal flow rate by adjusting compressor RPM and openings of air supply valves.

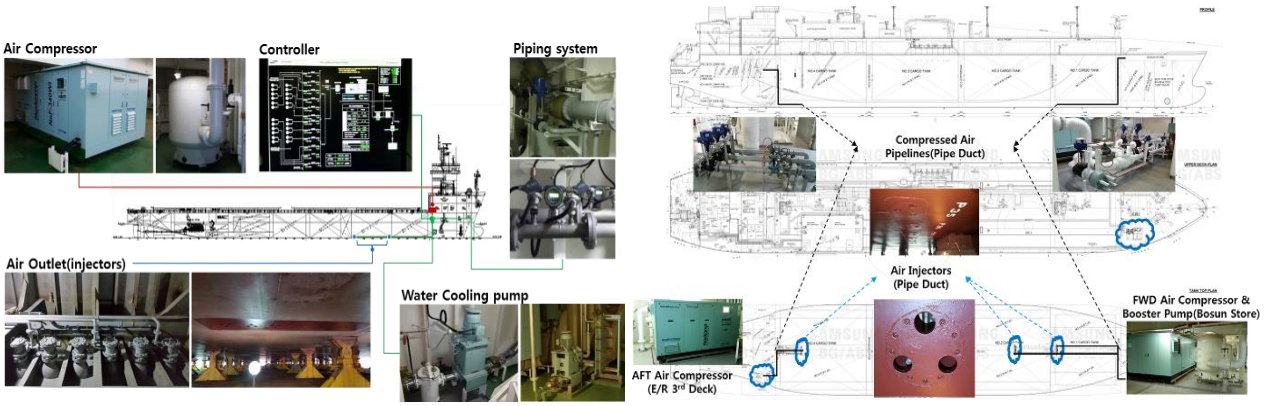

(a) HCC (b) LNGC

Figure 13: Arrangement of ALS for HCC and LNGC

3.2 Air Compressor

The specifications of the installed air compressor summarized in Table 5 were based on the optimal air injection flow rate obtained from the model tests. An inverter was installed to minimize the power consumption by adjusting the rotation speed of the driving motor according to specified air injection flow rate. The maximum outlet pressure was selected considering hydrostatic pressure and pipe friction losses corresponding to the draught of each ship. The loss of HCC compressor was somewhat overestimated compared to that of LNGC, since HCC's air compressor was selected prior to a detail design stage due to its long lead time.

Table 5: Particulars of Air compressors

Item / Vessel	HCC	LNGC
Design Draught	5.3m	11.5m
Installed Location	Upper deck	Bosun store / Engine room
Max. Pressure	2.5 barg	2.0 barg
Type	Screw	Screw

3.3 Air Injectors

Air injectors were devised to inject air in a stable manner and make installation process easy even when they were to be installed during retrofit work. In order to investigate the effects of the ship motion depending on the shape of air injectors, an experiment was conducted to compare stand-alone type air injectors installed in a row (refer to Fig. 13) with single rectangular chamber types of air injector in which all injection holes were placed in a row. In Fig. 14, air flow patterns are compared according to the type of air injectors under the condition of a flow velocity of 1 m/s, an air flow rate of 100 SLPM (Standard Liter Per Minute) and a horizontal slope of ± 3 °. With the single rectangular chamber type of an air injector, air is biased toward one side due to the water pressure difference in the beam direction resulted from roll motion. On the other hand, it is noted that air is injected more uniformly and stably from the stand-alone type of an air injector. In addition, the stand-alone type of air injectors can be installed between existing longitudinal stiffeners as displayed in Fig. 13, which makes it easy to install them even during retrofit work.

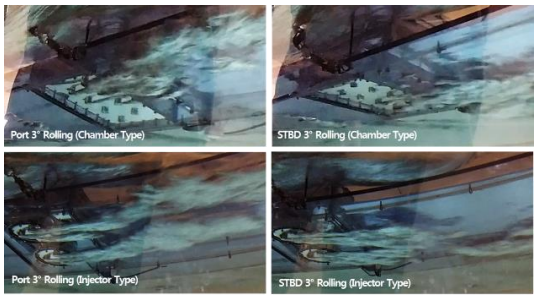

Figure 14: Behaviour of air depending on ship roll motion


Figure 15: Air injectors on the hull bottom

Figure 15 illustrates the pictures of the air injectors installed on the LNGC designed to be open and closed on the bottom hull for maintenance purpose. Aluminum anodes are installed and anti-fouling and corrosion paint is applied inside the air injectors to prevent fouling from marine growth.

4 REAL SHIP APPLICTION & VERIFICATION

4.1 Performance Evaluation of Real Ship for Heavy Cargo Carrier

To evaluate the power saving effect of the application of the ALS, a sea trial was carried out near Tsushima Island in October 2015. In order to minimize the influence of currents, a double run was conducted with the ALS turned on and off. DGPS and torsion meter were installed in addition to the ship's existing instruments to ensure the reliability of the measurements. The influence of wind and waves measured at the sea trial was corrected through the speed-power analysis in accordance with ISO15016-2015.

After HCC was retrofitted to install the ALS, a preliminary sea trial was carried out to confirm actual performance at the optimal air flow rate which had been determined through the model tests. The opening and closing rates of the injection control valves were adjusted so as to satisfy the ideal air layer thickness. In an attempt to evaluate the net power saving depending on the total air flow rate, measurements were made by decreasing the total air flow rate starting from the optimal flow rate (100%), while the ratio of air flow rate between FWD1 and FWD2 remained unchanged with the value determined from the model test results. Figure 16 shows the tendency of the net power saving to increase with the total air flow rate of the full scale

ship, which is similar to the model test results in Fig. 7. The reduction of net power saving at 100% flow rate seemed to be a local phenomenon stemming from environmental condition of the sea trial.

The ratio of the ideal air layer thicknesses between FWD1 and FWD2 was adjusted at a later stage to find the optimum during the preliminary sea trial, leading to the same value with the model test. From the observations at the preliminary sea trial above, the main sea trial was performed under the condition of 100% total air flow rate and the ratio of air layer thicknesses obtained from the model test. Other conditions of the sea trial are specified in Table 6.

Table 6: Sea trial conditions (HCC)

Item	Condition	Value / Unit
Draught	Ballast	4.7 m
Sea State	BF 4~5	1.0~1.5 m (Wave Height)
M/E Load	50 / 75 100	% MCR

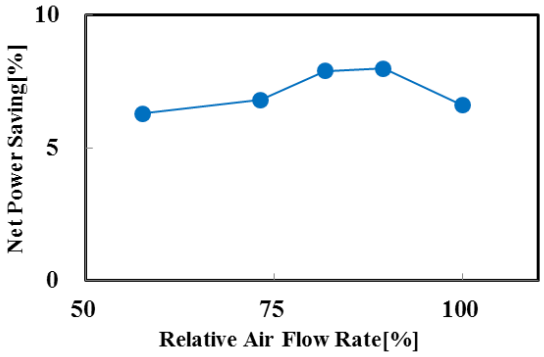

Figure 16: Effect of total air flow rate on net power saving

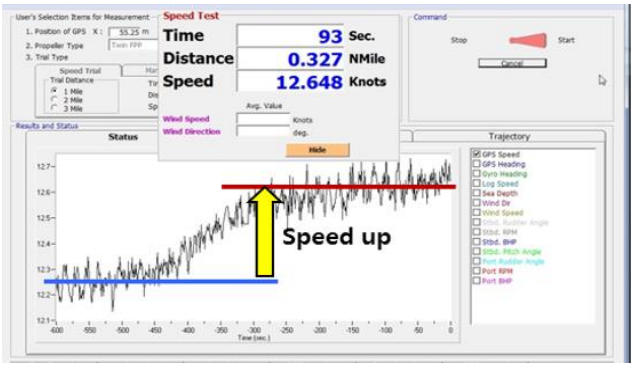

Figure 17: Increase of ship speed by ALS (HCC)

The effect of the ALS can be clearly seen in the results of the sea trial such as the increase of ship speed in Fig. 17 and reduction of shaft power in Fig. 18, respectively. The final result of the sea trial, summarized in Table 7, shows that the reduction of shaft power is 11.8%, and the net power saving is estimated to be 8.8% considering 3% of power consumed for air injection, which is slightly lower than the result of the model test.

Table 7: Sea trial conditions (HCC)

Ship Speed	12knots	13knots	Average
Shaft Power Reduction	12.9 %	10.7 %	11.8 %
Consumed Power for Air Compressor	3.3 %	2.7 %	3.0 %
Net Power Saving	9.6 %	8.0 %	8.8 %

※ Based on the shaft power with ALS OFF

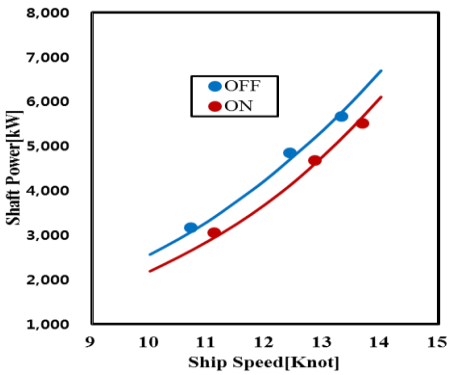

Figure 18: Speed-power performance obtained from sea-trial

4.2 Performance Evaluation of Real Ship for LNG Carrier

During the re-docking period for two-week, ALS was installed for retrofit of the 170K LNG carrier, and commissioning of the relevant equipment was completed. A sea trial at ballast draught was conducted near Sembawang shipyard in Singapore in December 2015 as per ISO15016: 2015 (E) procedure. In order to compensate for the influence of currents and directly compare the changes in speed and power in ALS ON and OFF conditions, the operation of ALS was carried out as shown in Fig. 19. A double run was executed in the order of ALS OFF/ON with engine load 50%, 75% and 90% MCR, respectively.

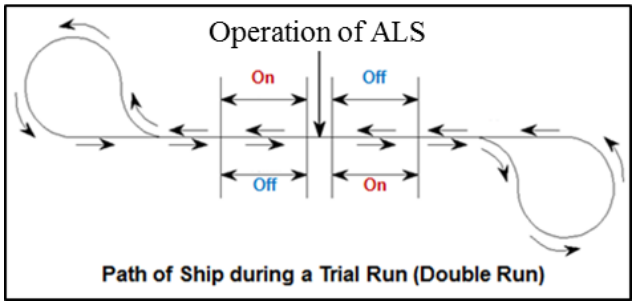

Figure 19: Path of ship and operation mode of ALS during sea trial

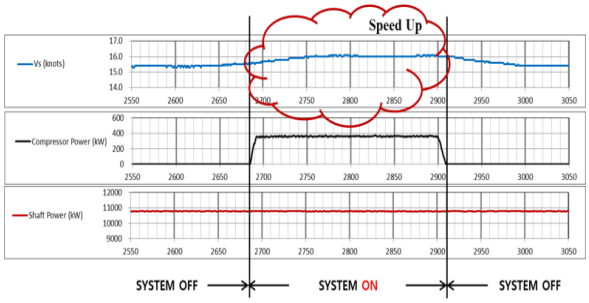

Figure 20: Increase of ship speed by ALS (LNGC)

A preliminary sea trial was carried out in a similar way to HCC, and the optimal total flow rate and air layer thickness ratio of each row of air injectors were investigated on the LNGC. Optimization was limited due to tight sea trial schedule, but the measured optimal conditions of total flow rate and air layer thickness ratio were different from those of the model test. The optimum total flow rate of the full scale ALS was increased by around 20% relative to the model test result and the flow rate ratio was measured to be 1:2.4:1.2 at FWD1, FWD2 and AFT1, respectively.

The sea trial was carried out at ballast draught under the condition determined from the preliminary sea trial. Figure 20 shows the time series variation of ship speed, compressor power and shaft power. It is clearly observed that ship speed and compressor power increases when ALS was turned on, while shaft power remains unchanged.

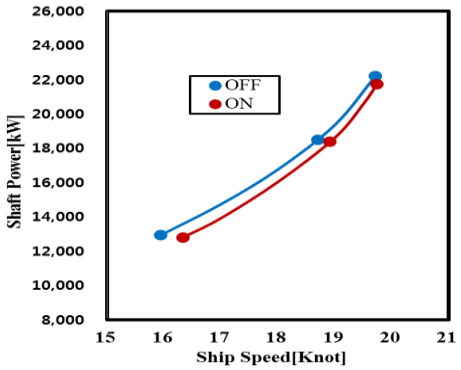

Figure 21: ALS effect on speed-power performance

Figure 21 shows the comparison of the speed-power curves corrected in accordance with ISO15016: 2015 (E) procedure when ALS is turned on and off. The shaft power saving was about 5.3% at the speed of 17.5 knots, and considering the power required for the air compressor, the net power saving was estimated to be about 3.2%, which is much lower than the model test result.

After the sea trial at ballast draught, additional optimization of the ALS operating condition was made at laden draught on a voyage in service from Gladstone, Australia to Inchon, Korea. Since the double run could not be carried out on the voyage, the power savings depending on the flow rate of each row of injectors (i.e. FWD1, FWD2 and AFT1) were repeatedly measured under the similar environmental conditions of wind, waves, and currents. Figure 22 shows the shaft power reductions at various total air flow rates relative to the flow rate applied at the sea trial (100%). It is observed that the power saving is increased as the total air flow rate is increased even at 100% or more. The ratio of the air layer thicknesses was, therefore,

optimized again to be 1:3:1.4 at the total flow rate with maximum power reduction, which gave rise to 4 ~ 5% of net power savings as shown in Fig. 23.

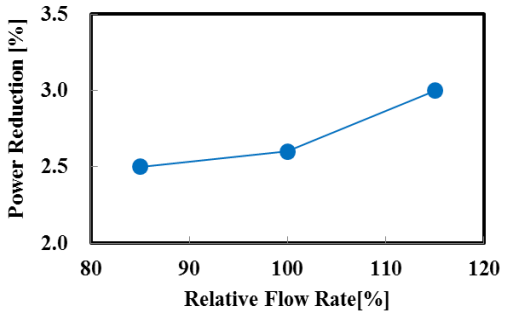

Figure 22: Power reduction depending on air flow rate at FWD2 air injectors

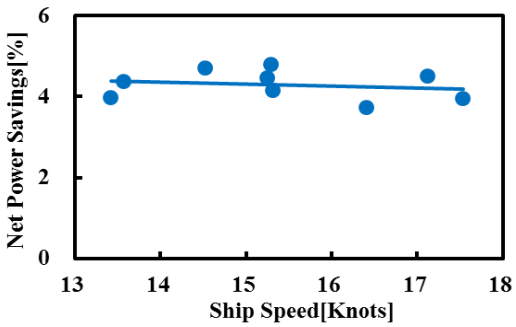

Figure 23: Net power savings for LNGC (Laden)

5 RESULTS: MODEL-SHIP CORRELATION

Performance evaluation and design optimization of the ALS were carried out through resistance and self-propulsion tests, assuming that the air layer thickness of model and full scale were the same. When evaluating the performance of the full scale ships, it is further assumed that the ratio of frictional resistances in model scale and full scale was kept the same regardless of the presence or absence of air injection as in Eq. (6). However, as can be seen in Table 8, the model test results based on these assumptions seemed to overestimate the rate of shaft power reduction compared to the sea trial results. Therefore, in order to improve the estimation accuracy of the power saving of the ALS based on the model test results, it is necessary to study in more detail the correlation of the reduction rate of the frictional resistance by air injection in model scale with that in full scale, including similarities of air layer thickness and diverging angle of air flow injected under the hull.

Since the air layer thicknesses of model and full scale were assumed to the same, the scale of real ship hull roughness relative to the air layer thickness would be significantly larger than that of the model ship. Therefore, the air layer of full scale ship seemed hardly remain stable and some area of the hull could not be covered by air.

Table 8: Comparison of model and real ship test results

Item / Vessel		**HCC**	**LNGC**
Condition		Ballast	Laden
Ship Speed [knots]		12.0	17.5
Model Ship Test	Air Layer Thickness Ratio	1:4.25	1:1.8:1
	Shaft Power Reduction [%]	24.5	9.0
Real Ship Test	Air Layer Thickness Ratio	1:4.25	1:3:1.4
	Shaft Power Reduction [%]	12.9	6.5

6 ADDITIONAL RESEARCH

As described above, the diverging angle is a factor that causes the performance difference between the model and full scale ship for the air lubrication system. For further verification of this, an air injector having the same shape as the real ship was prepared and the diverging angle test was performed with each flow velocity and air flow rate. The test was conducted at the cavitation tunnel in the SSMB and the system configuration is as shown in Fig. 24. The flow velocity conditions of the tunnels were selected from 2 m/s, which is equivalent to the model ship test, to 8 m/s, which corresponds to 17knots of the LNG Carrier operation speed. The air flow rate conditions were also selected to cover the actual flow rate in the model ship test and the flow conditions in the real ship test of two types of vessels. The test was carried out with

varying flow rate for each speed. The magnitude of the diverging angle shown in Fig. 25 is the measurement value of the angle of the air layer diffused from the point where the air was injected to the rear 7 m [9].

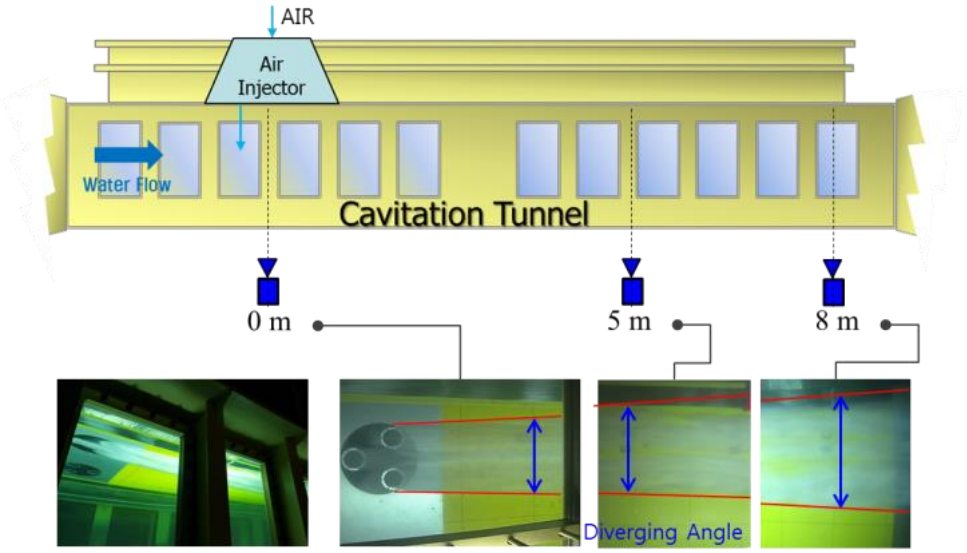

Figure 24: System configuration of diverging angle test

Table 9: Sea trial conditions (HCC)

Water Speed [m/s]	Air Flow Rate [m^3/h]	Remark
2	23~300	Model ship test condition
4	30~256	-
6	17~318	Real ship condition (HCC)
8	17~315	Real ship condition (LNGC)

As explained in the previous, it can be seen that the results in case of 2m/s, which corresponds to the model ship test condition, shows a small diverging angle at the low flow rates. At 6m/s which corresponding to HCC, it was confirmed that the diverging angle was 6 degrees maximum and at 200m^3/h or more, the diverging angle did not increase any more. It can be seen that the diverging angle of 8m/s corresponding to LNGC also has a maximum diverging angle of 4 degrees, and it was evaluated that the diverging angle does not increase more than 180m^3/h. In conclusion, it was found that the diverging angle increases with increasing air flow rate or slower flow velocity. In addition, it can be seen that as the flow velocity increases, the flow rate reaching the maximum diffusion angle becomes smaller.

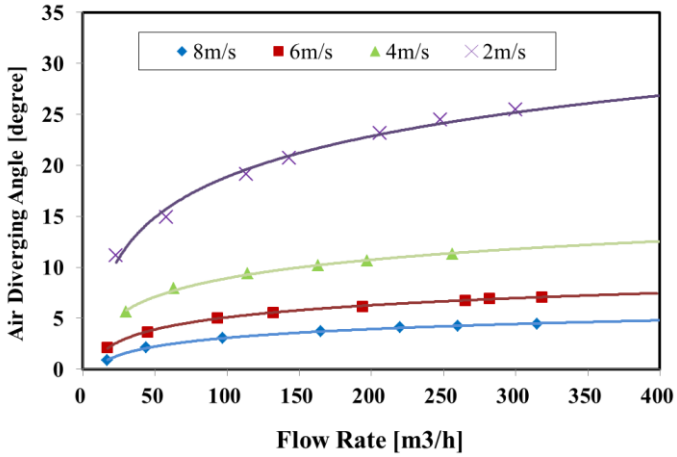

Figure 25: Diverging angle with flow velocity and air flow rate

7 CONCLUSION

The ALS of HCC has been estimated to have the net power saving of 8.8% according to the sea trial result, and that of LNGC retrofit has about 4 ~ 5% net power saving during long term voyages in service. The rates of shaft power reduction by the ALS evaluated through the sea trials are less than that estimated by the model tests, which is presumed to be resulted from the difference in frictional resistance reduction ratios in model scale and full scale. Therefore, further research should be undertaken to understand the scale effect of air layer on the reduction of frictional resistance.

According to the results of ongoing research efforts, it seems to be possible to further optimize the design and operating conditions of the ALS to achieve more than 6% of net power saving for contemporary twin skeg LNGCs.

ACKNOWLEDGEMENTS

This work was carried out in the research grant, Development of air lubrication systems to reduce ship's fuel consumption about 5% and verification of the performance in real sea [10073164], supported by the Ministry of Trade, Industry and Energy of Korea.

REFERENCES

[1] Bushnell, D.M. & Hefner, J.N., "Viscous Drag Reduction in Boundary Layers". in: *Progress in Astronautics and Aeronautics*, Vol 123, (The American Institute of Aeronautics and Astronautics, Inc., Washington, DC, USA, 1990)

[2] Elbing, B.R., Winkel, E.S., Lay, K.A., Ceccio, S.L., Dowling, D.R., and Perlin, M. In: "Bubble-Induced Skin Friction Drag Reduction and the Abrupt Transition to Air-Layer Drag Reduction", *J. Fluid Mechanics*, Vol 612, pp 201-236, 2008.

[3] Jang, J. H. et al, "Experimental investigation of frictional resistance reduction with air layer on the hull bottom of a ship". In: *IJNAOE*, Vol 2, No 6, pp 363-379, 2014

[4] Pinches, M.J. & Callear, B.J., *Power Pneumatics*, Prentice Hall, pp 19-22, 1996

[5] Ceccio, S. L. & Mäkiharju, S. A. *Air Lubrication Drag Reduction on Great Lakes Ships*. Dept. Naval Architects and Marine Engineering (Univ. of Michigan, 2012)

[6] Mäkiharju, S., Perlin, M., and Ceccio, S., "On the Energy Economics of Air Lubrication Drag Reduction". In: *International Journal of naval architecture and Ocean Engineering*, Vol 4, No 4, pp 412-422, 2012

[7] Kim S.M., Kim J.J., Choi S.H., Kim J.J., Lee J.D., Lee D.Y., Kim B.K., "Development and Performance Optimization of Air Lubrication System for a Ship". In: *Proceedings of the Annual Spring Meeting of the Society of Naval Architects of Korea*, Busan, Republic of Korea, 2017

[8] Kim J.H., Kim J.J., Kim S.M., Kim J.K., Choi S.H., Lee D.Y., Kim B.K., "A study of full scale application of Samsung`s air lubrication system (SAVER Air) for an LNG carrier". In: *Proceedings of the Annual Spring Meeting of the Society of Naval Architects of Korea*, Busan, Republic of Korea, 2017

[9] Kim S.M., Kim J.J., Choi S.H., Lee D.Y., "Experimental investigation of the characteristics of air layer on the flat plate by air flow rate and injection type". In: *Proceedings of the Annual Autumn Meeting of the Society of Naval Architects of Korea*, Changwon, Republic of Korea, 2018